THE PAMELA COSMIC RAY SPACE OBSERVATORY: DETECTOR, OBJECTIVES and FIRST RESULTS

Marco Casolino* Daniel Bongue, Maria Pia De Pascale, Nicola De Simone
Valeria Di Felice Laura Marcelli Mauro Minori
Piergiorgio Picozza, Roberta Sparvoli
INFN and Physics Department of University of Rome "Tor Vergata"
* *Corresponding author: casolino@roma2.infn.it*
Guido Castellini
IFAC, Florence, Italy
Oscar Adriani, Lorenzo Bonechi, Massimo Bongi
Sergio Bottai Paolo Papini, Sergio Ricciarini
Piero Spillantini, Elena Taddei, Elena Vannuccini
INFN, and Physics Department of University of Florence
Giancarlo Barbarino, Donatella Campana, Rita Carbone
Gianfranca De Rosa, Giuseppe Osteria
INFN, and Physics Department of University of Naples "Federico II"
Mirko Boezio, Valter Bonvicini, Emiliano Mocchiutti, Andrea Vacchi
Gianluigi Zampa, Nicola Zampa
INFN, and Physics Department of University of Trieste
Alessandro Bruno, Francesco Saverio Cafagna
INFN, and Physics Department of University of Bari
Marco Ricci
INFN, Laboratori Nazionali di Frascati, Italy
Petter Hofverberg, Mark Pearce, Per Carlson
KTH, Stockholm, Sweden
Edward Bogomolov, S.Yu. Krutkov, N.N. Nikonov, G.I.Vasilyev
Ioffe Physical Technical Institute, St. Petersburg, Russia
Wolfgang Menn, Manfred Simon
Universität Siegen, Germany
Arkady Galper, Lubov Grishantseva, Sergey Koldashov, Alexey Leonov
Vladimir V. Mikhailov, Sergey A. Voronov, Yuri T. Yurkin, Valeri G. Zverev
Moscow Engineering and Physics Institute, Moscow, Russia
Galina A. Bazilevskaya, Alexander N. Kvashnin
Osman Maksumov, Yuri Stozhkov
Lebedev Physical Institute, Moscow, Russia

Abstract

PAMELA is a satellite borne experiment designed to study with great accuracy cosmic rays of galactic, solar, and trapped nature in a wide energy range (protons: 80 MeV-700 GeV, electrons 50 MeV-400 GeV). Main objective is the

study of the antimatter component: antiprotons (80 MeV-190 GeV), positrons (50 MeV-270 GeV) and search for antimatter with a precision of the order of 10^{-8}). The experiment, housed on board the Russian Resurs-DK1 satellite, was launched on June, 15 2006 in a 350×600 km orbit with an inclination of 70 degrees. The detector is composed of a series of scintillator counters arranged at the extremities of a permanent magnet spectrometer to provide charge, Time-of-Flight and rigidity information. Lepton/hadron identification is performed by a Silicon-Tungsten calorimeter and a Neutron detector placed at the bottom of the device. An Anticounter system is used offline to reject false triggers coming from the satellite. In self-trigger mode the Calorimeter, the neutron detector and a shower tail catcher are capable of an independent measure of the lepton component up to 2 TeV. In this work we describe the experiment, its scientific objectives and the performance in its first two years of operation. Data on protons of trapped, secondary and galactic nature - as well as measurements of the December 13 2006 Solar Particle Event - are provided.

Essentially a pre-antiparticle measurement paper.
Invited talk in *La Thuile 2008*, Les Rencontres de Physique de la Vallée d'Aoste. *Results and Perspectives in Particle Physics.*
24 February 2008 - 01 March 2008

1 Introduction

The Wizard collaboration is a scientific program devoted to the study of cosmic rays through balloon and satellite-borne devices. Aims involve the precise determination of the antiproton[1] and positron[2] spectrum, search of antimatter, measurement of low energy trapped and solar cosmic rays with the NINA-1 [3] and NINA-2[4] satellite experiments. Other research on board Mir and International Space Station has involved the measurement of the radiation environment, the nuclear abundances and the investigation of the Light Flash[5] phenomenon with the Sileye experiments[6 7]. PAMELA is the largest and most complex device built insofar by the collaboration, with the broadest scientific goals. In this work we describe the detector, and its launch and commissioning phase. Scientific objectives are presented together with the report of the first observations of protons of solar, trapped and galactic nature.

2 Instrument Description

In this section we describe the main characteristics of PAMELA detector; a more detailed description of the device and the data handling can be found in[8910]. The device (Figure 1) is constituted by a number of highly redundant detectors capable of identifying particles providing charge, mass, rigidity

and beta over a very wide energy range. The instrument is built around a permanent magnet with a silicon microstrip tracker with a scintillator system to provide trigger, charge and time of flight information. A silicon-tungsten calorimeter is used to perform hadron/lepton separation. A shower tail catcher and a neutron detector at the bottom of the apparatus increase this separation. An anticounter system is used to reject spurious events in the off-line phase. Around the detectors are housed the readout electronics, the interfaces with the CPU and all primary and secondary power supplies. All systems (power supply, readout boards etc.) are redundant with the exception of the CPU which is more tolerant to failures. The system is enclosed in a pressurized container (Figure 2,3) located on one side of the Resurs-DK satellite. In a twin pressurized container is housed the Arina experiment, devoted to the study of the low energy trapped electron and proton component. Total weight of PAMELA is 470 kg; power consumption is 355 W, geometrical factor is $21.5 cm^2 sr$.

2.1 Resurs-DK1 Satellite

The Resurs-DK1 satellite (Figure 2) is the evolution of previous military reconnaissance satellites flown during in the years 1980 - 1990. It was developed by TsSKB Progress plant[11] in the city of Samara (Russia), in cooperation with NPP OPTEKS, OAO Krasnogorskiy Zavod, NIITP and NTsOMZ (Russia's Science Center for Remote Sensing of Earth)[12]. The spacecraft is three-axis stabilized, with axis orientation accuracy 0.2 arcmin and angular velocity stabilization accuracy of 0.005^o/s. The spacecraft has a mass of about 6650 kg, height of 7.4 m and a solar array span of about 14 m. It is designed to provide imagery of the Earth surface for civilian use and is the first Russian non-military satellite with resolution capability of $\simeq$ 0.8 m in composite color mode[1]. The imaging system has a coverage area at 350 km of 28.3 448 km, obtained with oscillation of the satellite by 30^o in the cross-track direction. Onboard memory capacity is 769 Gbit. The RF communications for the payload data are in X-band at 8.2-8.4 GHz with a downlink data rate of 75, 150 and 300 Mbit/s. PAMELA data amounts to about 16 Gbyte/day, sent to ground and processed in NTsOMZ station in Moscow, where also the data analysis and quicklook procedures for PAMELA are performed.

2.2 Scintillator / Time of Flight system

The scintillator system[13] provides trigger for the particles and time of flight information for incoming particles. There are three scintillators layers, each

[1]Observations are performed in three bands (0.50 - 0.60μm , 0.60 - 0.70μm, 0.70 - 0.80μm) each with 2.5-3.5 m resolution to produce a composite color image.

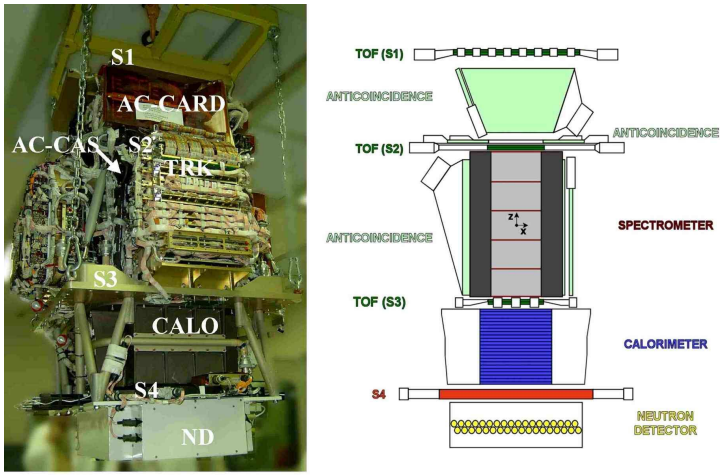

Figure 1: Left: Photo of the PAMELA detector during the final integration phase in Tor Vergata clean room facilities, Rome. It is possible to discern, from top to bottom, the topmost scintillator system, S1, the electronic crates around the magnet spectrometer, the baseplate (to which PAMELA is suspended by chains), the black structure housing the Si-W calorimeter, S4 tail scintillator and the neutron detector. Right: scheme - approximately to scale with the picture - of the detectors composing PAMELA .

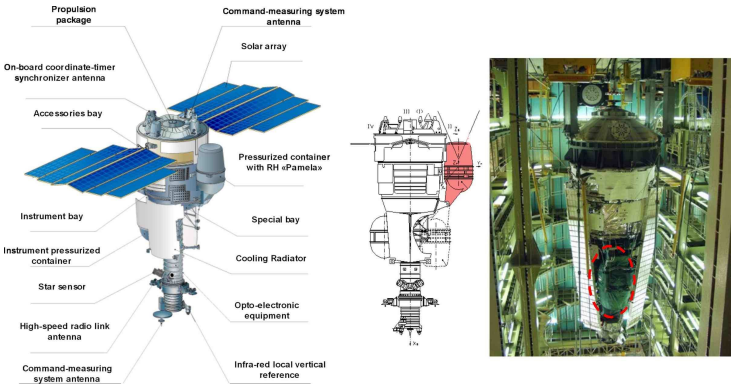

Figure 2: Left: Scheme of the Resurs-DK1 satellite. PAMELA is located in the pressurized container on the right of the picture. In the center panel it is possible to see the container in the launch position and in the extended (cosmic ray acquisition) configuration. In the right panel it is possible to see a picture of the satellite in the assembly facility in Samara. The picture is rotated 180 degrees to compare the photo with the scheme. The dashed circle shows the location of PAMELA pressurized container in the launch position.

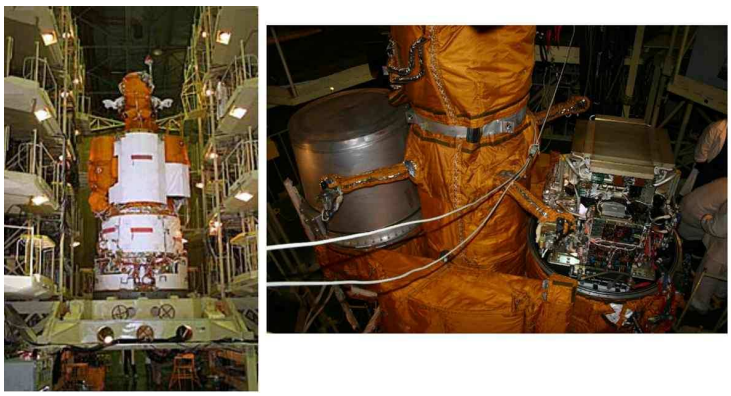

Figure 3: Left: Photo of Resurs in the final integration phase in Baikonur. It is possible to discern the the optical sensor on top, the two pressurized containers on the sides, and the white heat cooling panel in the forefront. Right: close up picture of the integration phase of PAMELA in the pressurized container (right in picture).

composed by two orthogonal planes divided in various bars (8 for S11, 6 for S12, 2 for S21 and S12 and 3 for S32 and S33) for a total of 6 planes and 48 phototubes (each bar is read by two phototubes). S1 and S3 bars are 7 mm thick and S2 bars are 5 mm. Interplanar distance between S1-S3 of 77.3 cm results in a TOF determination of 250 ps precision for protons and 70 ps for C nuclei (determined with beam tests in GSI), allowing separation of electrons from antiprotons up to $\simeq 1$ GeV and albedo rejection. The scintillator system is also capable of providing charge information up to $Z = 8$.

2.3 Magnetic Spectrometer

The permanent magnet [14] is composed of 5 blocks, each divided in 12 segments of Nd-Fe-B alloy with a residual magnetization of 1.3 T arranged to provide an almost uniform magnetic field along the y direction. The size of the cavity is $13.116.144.5\,cm^3$, with a mean magnetic field of 0.43 T. Six layers of $300\mu\,m$ thick double-sided microstrip silicon detectors are used to measure particle deflection with 3.00.1 μm and 11.50.6 μm precision in the bending and non-bending views. Each layer is made by three ladders, each composed by two $5.337.00\,cm^2$ sensors coupled to a VA1 front-end hybrid circuit. Maximum Detectable Rigidity (MDR) was measured on CERN proton beam to be $\simeq 1TV$.

2.4 Silicon Tungsten Calorimeter

Lepton/Hadron discrimination is performed by the Silicon Tungsten sampling calorimeter [15] located on the bottom of PAMELA . It is composed of 44 silicon layers interleaved by 22 0.26 cm thick Tungsten plates. Each silicon layer is composed arranging 33 wafers, each of $80 \times 80 \times .380\,mm^3$ and segmented in 32 strips, for a total of 96 strips/plane. 22 planes are used for the X view and 22 for the Y view in order to provide topological and energetic information of the shower development in the calorimeter. Tungsten was chosen in order to maximize electromagnetic radiation lengths (16.3 X_o) minimizing hadronic interaction length (0.6 λ_{int}). The CR1.4P ASIC chip is used for front end electronics, providing a dynamic range of 1400 mips (minimum ionizing particles) and allowing nuclear identification up to Iron.

2.5 Shower tail scintillator

This scintillator ($48\times48\times1\,cm^3$) is located below the calorimeter and is used to improve hadron/lepton discrimination by measuring the energy not contained in the shower of the calorimeter. It can also function as a standalone trigger for the neutron detector.

2.6 Neutron Detector

The $60 \times 55 \times 15 cm^3$ neutron detector is composed by 36 ^3He tubes arranged in two layers and surrounded by polyethylene shielding and a 'U' shaped cadmium layer to remove thermal neutrons not coming from the calorimeter. It is used to improve lepton/hadron identification by detecting the number of neutrons produced in the hadronic and electromagnetic cascades. Since the former have a much higher neutron cross section than the latter, where neutron production comes essentially through nuclear photofission, it is estimated that PAMELA overall identification capability is improved by a factor 10. As already mentioned, the neutron detector is used to measure neutron field in Low Earth Orbit and in case of solar particle events as well as in the high energy lepton measurement.

2.7 Anticoincidence System

To reject spurious triggers due to interaction with the main body of the satellite, PAMELA is shielded by a number of scintillators used with anticoincidence functions[16,17]. CARD anticoincidence system is composed of four 8 mm thick scintillators located in the area between S1 and S2. CAT scintillator is placed on top of the magnet: it is composed by a single piece with a central hole where the magnet cavity is located and read out by 8 phototubes. Four scintillators, arranged on the sides of the magnet, make the CAS lateral anticoincidence system.

3 Integration, Launch and Commissioning

Pamela was integrated in INFN - Rome Tor Vergata clean room facilities; tests involved first each subsystem separately and subsequently the whole apparatus simulating all interactions with the satellite using an Electronic Ground Support Equipment. Final tests involved cosmic ray acquisitions with muons for a total of about 480 hours. The device was then shipped to TsKB Progress plant, in Samara (Russia), for installation in a pressurized container on board the Resurs-DK satellite for final tests. Also in this case acquisitions with cosmic muons (140 hours) have been performed and have shown the correct functioning of the apparatus, which was then integrated with the pressurized container and the satellite. The detector was then dismounted from the satellite and shipped by air to Baikonur cosmodrome (Kazakstan) where the the final integration phase took place in 2006.
The Soyuz-U rocket was launched from Baikonur Cosmodrome Pad 5 at Site 1, the same used for manned Soyuz and Progress cargoes to the International Space Station. Launch occurred on June 15^{th} 2006, 08:00:00.193 UTC with the payload reaching orbit after 8 minutes. Parking orbit had a semimajor

axis of 6642 km. Final boost occurred on June 18^{th} 2006 when the orbit was raised with two engine firings to a semimajor axis of 6828 km. The maneuver was completed before 17:00 Moscow time. The transfer orbit resulted in a height increase from 198×360 km to 360×604 km, with the apogee of the lower orbit becoming perigee of the final orbit. Also inclination of the satellite (Figure 5) was increased from 69.93^o to $\simeq 69.96^o$. In the same Figure it is also possible to see long term variations of 0.1^o in a period of 5 months due to the oblateness of the Earth. In Figure 4 it is possible to see the altitude of the satellite after launch, showing the final boost and the secular variation due to atmospheric drag, resulting in a decrease of the apogee of 10 km in 5 months and a corresponding increase of the number of revolutions/day (spacecraft velocity is inversely proportional to square root of height). To compensate for atmospheric drag, the altitude of the satellite is periodically reboosted by vernier engines. To perform this maneuver the pressurized container housing PAMELA is folded back in the launch position, the satellite is rotated 180^o on its longitudinal axis and then engines are started. Reboost frequency depends from orbital decay, due to atmospheric drag. Up to December 2006 the activity has been low with two small Solar Particle Events in summer and three larger events generated by sunspot 930 in December, so there has not been the need to perform this maneuver so far. In Figure 6 is shown the value of the angle (Beta angle) between the orbital plane and the Earth-Sun vector. This value should vary with a one-year periodicity but the oblateness of the Earth causes to precess with a higher frequency. The position of the orbital plane affects the irradiation and temperature of the satellite, which is - for instance - always under the Sun for high values of the absolute value of beta. These thermal excursions are greatly reduced in the pressurized container of PAMELA thanks to the cooling loop with a fluid at a temperature of $28 - 33^o$ which maintains the temperature of the detector relatively low and reduces fluctuations within some degrees.

As already mentioned Resurs-DK1 oscillates on its longitudinal axis when performing Earth observations: a detailed information of the attitude of the satellite is provided to the CPU of PAMELA in order to know the orientation of the detector with precision of $\simeq 1$ degree. Position and attitude information of the satellite are provided to PAMELA CPU via a 1553 interface (used also for Command and Control) and are based on the GLONASS (GLObal Navigation Satellite System), similar to the GPS positioning system.
On June 22, ground control successfully tested the Geoton-1 optical-electronic system and the Sangur-1 data receiving and processing system, according to Roskosmos. On June 23, 2006, NTsOMZ received first images from the satellite: the satellite conducted two photographic sessions, lasting five seconds each. On September 15, 2006, Roskosmos announced that testing of the spacecraft was successfully completed on that day and State Commission planned to convene on September 21, 2006, to declare the satellite operational. On September

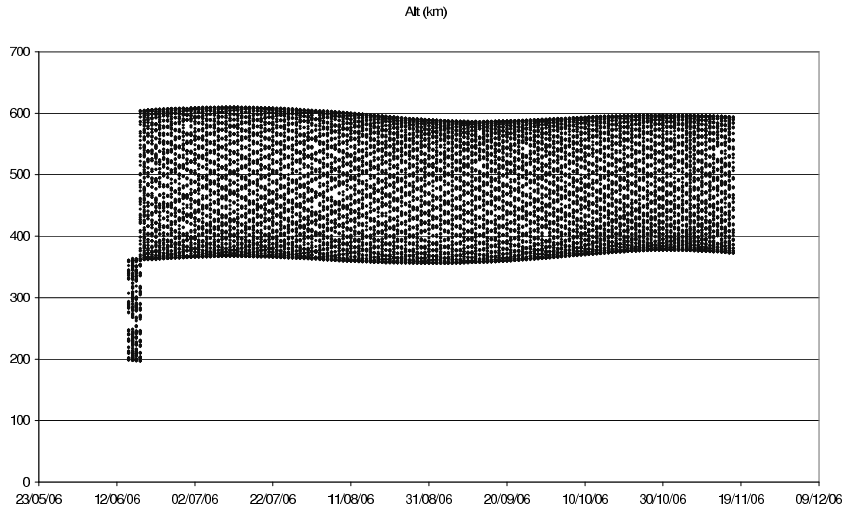

Figure 4: Height of Resurs as a function of time. After four days in a parking orbit with 198×360 km the orbit was boosted to 360×604 km. As of 17/11/2006 height has passed to 372 × 594 km.

22, 2006, Roskosmos confirmed that the spacecraft was declared operational as scheduled. Commissioning of the experiment proceeded in parallel with Resurs-DK1 and mostly consisted in a fine tuning of the observational parameters of PAMELA and the on board software, optimizing time and schedule of downlinks to maximize live time of the instrument.

4 In flight data and instrument performance in Low Earth Orbit

PAMELA was first switched on June, 26^{th} 2006. Typical events are shown in Figure 7 where an electron and a positron crossing the detector and being bent in different directions by the magnetic field are shown. In the third panel a proton interacting hadronically in the calorimeter is visible. Note that the two leptons have energies too low to give appreciable electromagnetic showers.

In Figure 8 are shown PAMELA world particle rate for S11*S12 at various altitudes (integral fluxes of $E > 35$ MeV p; $E > 3.5$ MeV e^-), showing the high latitude electron radiation belts and the proton belt in the South Atlantic Anomaly. Outside the SAA it is possible to see the increase of particle rate at the geomagnetic poles due to the lower geomagnetic cutoff. The highest rates are found when the satellite crosses the trapped components of the Van Allen Belts in agreement with AP-8 and AE-8 models for trapped radiation[18].

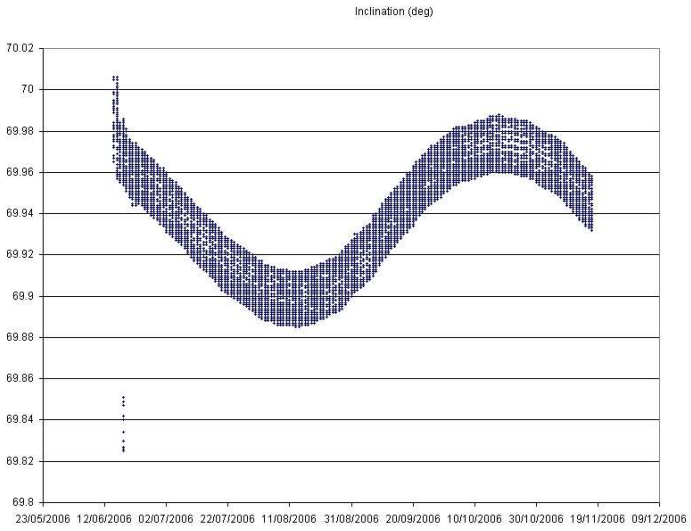

Figure 5: Inclination of Resurs satellite as a function of time. The final boost after launch increased inclination of the satellite. It is possible to see secular oscillation of $\simeq 0.1^o$ and short term (daily) variation of 0.03^o.

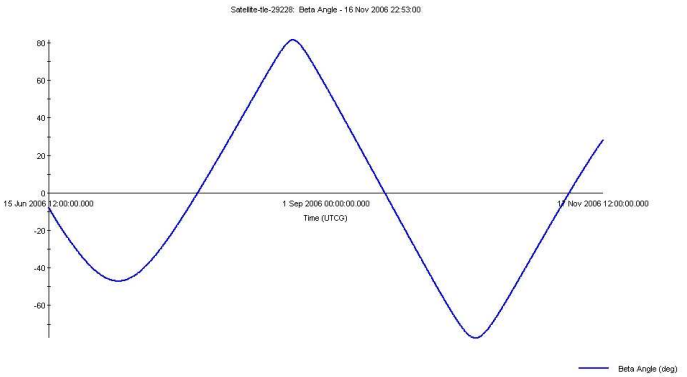

Figure 6: Beta angle of satellite vs time. The inclined orbit of the satellite and the oblateness of the Earth result in the precession of the node line resulting in a faster oscillation of the angle.

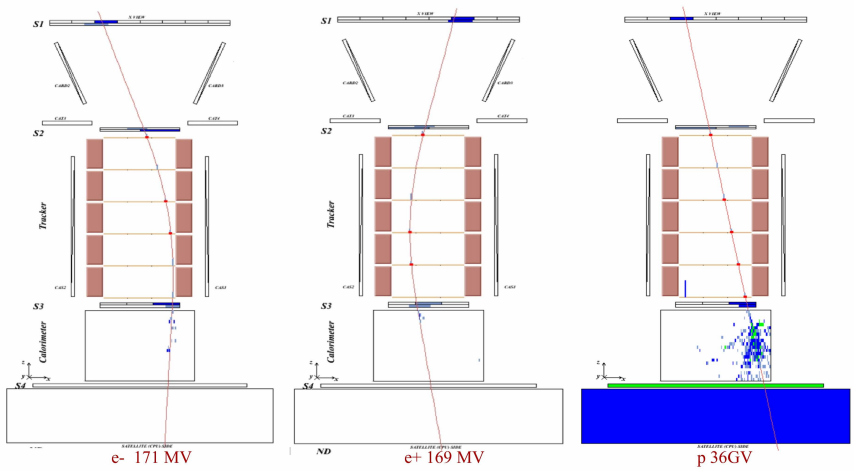

Figure 7: Some cosmic ray events observed with PAMELA . Left: 0.171 GV e^-. The particle enters the detector from the top hitting the two layers of S1 and the two layers of S2, located just above the magnet cavity. The trajectory is bent by the magnetic field and its rigidity is revealed by the microstrip detector of the tracker. The particle interacts with the bottom scintillator (S3) before absorption by the Si-W tracking calorimeter. Centre: 0.169 GV positron. Aside from the opposite curvature, the particle interacts as in the preceding case. Right: 36 GV proton. Its high rigidity reduces the magnet curvature. The calorimeter shows the shower from an hadronic interaction, with secondary particles hitting the shower tail scintillator (S4) and the neutron detector.

In Figure 9 is shown the $\beta = v/c$ of particles measured with the Time of Flight (TOF) system as function of the geographical latitude observed. It is possible to see the effect of geomagnetic cutoff on low energy particles, present only closer to the poles. Also the South Atlantic region, composed mostly of low energy ($E < 200MeV$), low β trapped protons is clearly seen at the latitudes between 40^o and 20^o S. Also albedo ($\beta < 0$) particles crossing the detector from the bottom to the top are shown in the plot. Note the absence of high energy albedo particles.

5 Scientific Objectives and first observations

PAMELA can perform a detailed measurement of the composition and energy spectra of cosmic rays of galactic, trapped and secondary nature in Low Earth

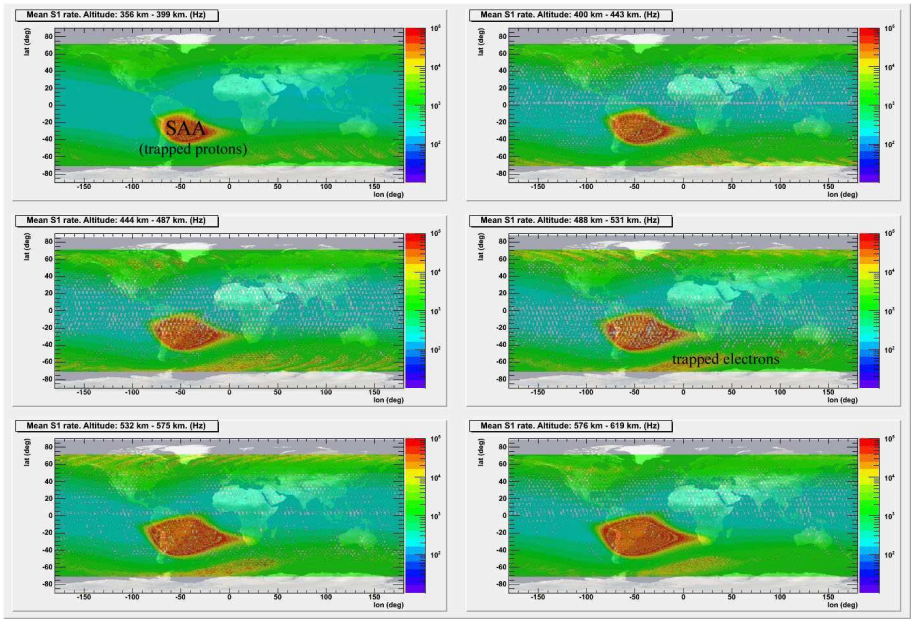

Figure 8: All particle map ($E > 35$ MeV p; $E > 3.5$ MeV e^-) measured at various altitudes with PAMELA . In it are visible the proton (equatorial) and electron (high latitude) radiation belts, regions of trapped particles where the flux can increase several orders of magnitude. The size of the belts increases with altitude where the weaker magnetic field is capable of trapping lower energy particles.

Orbit. Its 70^o, 350×600 km orbit makes it particularly suited to study items of galactic, heliospheric and trapped nature. Furthermore, the long duration of the mission and the orbit configuration should allow for studies of spatial and temporal dependence in solar quiet and active conditions[19][20][21]. Indeed for its versatility and detector redundancy PAMELA is capable to address at the same time a number of different cosmic ray issues ranging over a very wide energy range, from the trapped particles in the Van Allen Belts, to electrons of Jovian origin, to the study of the antimatter component. Figure 11 shows the different components of the cosmic ray particle and antiparticle fluxes with some of the PAMELA measurements. Galactic protons are dominant, with Solar Energetic and trapped particles being the only components more abundant, albeit in an interval of time and in a specific region of the orbit respectively. Here we

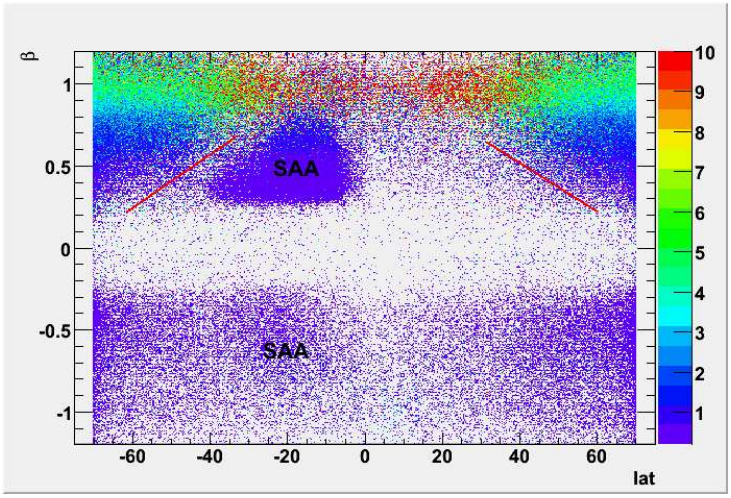

Figure 9: β vs geographical latitude of particles measured with PAMELA . Color code represents rigidity measured with the tracker. The red lines are to guide the eye and show the cutoff on galactic particles. High rigidity particles are present at all latitudes, whereas lower β events (mostly due to protons) are observed only at high latitudes and in the SAA.

briefly describe the main scientific objectives of the experiment and some of the preliminary results obtained up to now.

5.1 Antimatter research.

The study of the antiparticle component ($\overline{p}$, e^+) of cosmic rays is the main scientific goal of PAMELA . A long term and detailed study of the antiparticle spectrum over a very wide energy spectrum will allow to shed light over several questions of cosmic ray physics, from particle production and propagation in the galaxy to charge dependent modulation in the heliosphere to dark matter detection. In Figure 12 and 13 are shown the current status of the antiproton and positron measurements compared with PAMELA expected measurements in three years. In each case the two curves refer to a secondary only hypothesis with an additional contribution of a neutralino annihilation. Also cosmological issues related to detection of a dark matter signature and search for antimatter (PAMELA will search for $\overline{He}$ with a sensitivity of $\approx 10^{-8}$) will therefore be addressed with this device.

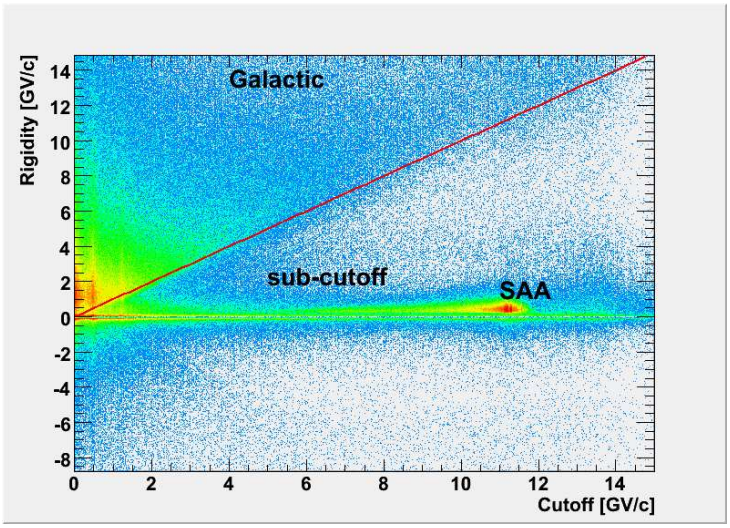

Figure 10: Rigidity vs Stormer Cutoff observed with PAMELA . Colour bar represents β of particles measured from the TOF. The effect of the geomagnetic field on galactic particles is clearly visible. Primary particles have an energy above the cutoff and are well separated from reentrant albedo events produced in the interaction of particles with the Earth's atmosphere.

5.1.1 **Antiprotons**

PAMELA detectable energy spectrum of $\overline{p}$ ranges from 80 MeV to 190 GeV. Although the quality of $\overline{p}$ data has been improving in the recent years, a measurement of the energy spectrum of $\overline{p}$ will allow to greatly reduce the systematic error between the different balloon measurements, to study the phenomenon of charge dependent solar modulation, and will for the first time explore the energy range beyond $\simeq$ 40 GeV. Possible excesses over the expected secondary spectrum could be attributed to neutralino annihilation;[434445] show that PAMELA is capable of detecting an excess of antiprotons due to neutralino annihilation in models compatible with the WMAP measurements. Also[46] estimate that PAMELA will be able to detect a supersymmetric signal in many minimal supergravity (mSUGRA) models. The possibility to extract a neutralino annihilation signal from the background depends on the parameters used, the boost factor (BF) and the galactic proton spectrum. Other scenarios[47 48] suppose the existence of heavy neutrinos or stable heavy particles as DM constituents. In [49] the preliminary results of PAMELA on $\overline{p}$are compared with other measure-

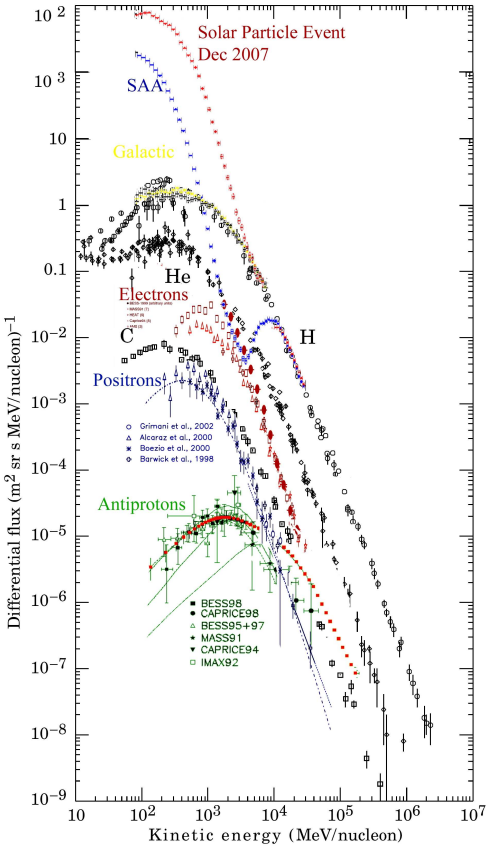

Figure 11: Differential energy spectra of the different particles detectable by PAMELA . Protons and Helium nuclei dominate the positive charge spectrum and electrons the negative charge spectrum. Antiparticles are extremely rare in cosmic rays, with positrons as abundant as Carbon nuclei. PAMELA acceptance energy range is 80 MeV - 190 GeV for antiprotons and 50 MeV - 270 GeV for positrons. On the experimental data for antiproton spectra is shown an expected contribution in case of a 964 GeV neutralino. Most intense fluxes refer to the trapped protons in the South Atlantic Anomaly and those coming from the December 13, 2006 Solar Particle event.

ments to explore the possibility of DM signature in fermion 3-plet ot 5-plet scenarios and conclude the possibility to extract a signal in case of BF=10.

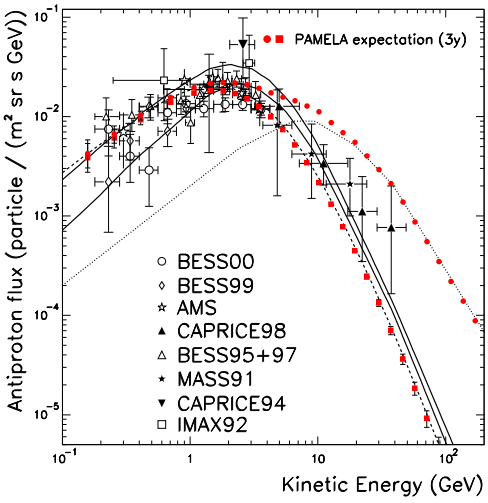

Figure 12: Recent experimental $\overline{p}$ spectra (BESS00 and BESS99 [22], AMS[23], CAPRICE98[24], BESS95+97[25], MASS91[26], CAPRICE94[1], IMAX92[27]) along with theoretical calculations for pure $\overline{p}$ secondary production (solid lines:[28], dashed line:[29]) and for pure $\overline{p}$ primary production (dotted line:[30], assuming the annihilation of neutralinos of mass 964 GeV/c^2). (Taken from[8])

Charge dependent solar modulation, observed with the BESS balloon flights at Sun field reversal[22] and more recently on a long duration balloon flight[50] will be monitored during the period of recovery going from the 23^{rd} solar minimum going to the 24^{th} solar maximum. Also the existence, intensity and stability of secondary antiproton belts[51], produced by the interaction of cosmic rays with the atmosphere will be measured.

5.1.2 **Positrons**

A precise measurement of the positron energy spectrum is needed to distinguish dark matter annihilation from other galactic sources such as hadronic production in giant molecular clouds, e^+/e^- production in nearby pulsars or decay from radioactive nuclei produced in supernova explosions. An interesting feature of e^+ is that - as electrons - they lose most of length scales of a few kiloparsecs (¡50). The cosmic positron spectrum is therefore a samples of only the local dark matter distribution[52]. PAMELA is capable to detect e^+ in the

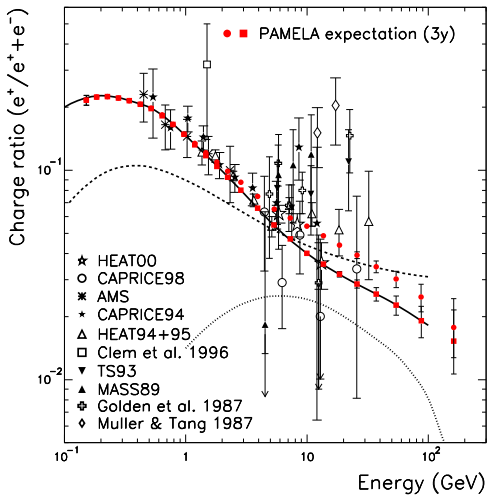

Figure 13: The positron fraction as a function of energy measured by several experiments ([313233] and MASS89[34], TS93[35], HEAT94+95[36], CAPRICE94[2], AMS[37], CAPRICE98[38], HEAT00[39]). The dashed[40] and the solid[41] lines are calculations of the secondary positron fraction. The dotted line is a possible contribution from annihilation of neutralinos of mass 336 GeV/c^2 [42]. The expected PAMELA performance, in case of a pure secondary component (full boxes) and of an additional primary component (full circles), are indicated in both panels. Only statistical errors are included in the expected PAMELA data. Taken from[8].

energy range 50 MeV to 270 GeV. Possibilities for dark matter detection in the positron channel depend strongly on the nature of dark matter, its cross section and the local inhomogeneity of the distribution. Hooper and Silk[53] perform different estimation of PAMELA sensitivity according to different hypothesis of the dark matter component: detection is possible in case of an higgsino of mass up to 220 GeV (with BF=1) and to 380 GeV (with BF=5). Kaluza Klein models[54] would give a positron flux above secondary production increasing above 20 GeV and thus clearly compatible with PAMELA observational parameters. In case of a bino-like particle, as supposed by Minimal Supersymmetric Standard Model, PAMELA is sensible to cross sections of the order of $2 - 3 \times 10^{-26}$ (again, depending of BF). In case of Kaluza Klein excitations of the Standard Model the sensitivity of PAMELA is for particles up to 350

and 550 GeV. In the hypothesis of the littlest Higgs model with T parity, the dark matter candidate is a heavy photon which annihilates mainly into weak gauge bosons in turn producing positrons. In[55] is shown that PAMELA will be able to identify this signal if the mass of the particle is below 120 GeV and the BF is 5. Hisano et al.,[56] assume a heavy wino-like dark matter component, detectable with PAMELA in the positron spectrum (and with much more difficulty in the antiproton channel) for mass of the wino above 300 GeV. This model predicts that if the neutralino has a mass of 2 TeV the positron flux increases by several orders of magnitude due to resonance of the annihilation cross section in W^+W^- and ZZ: in this scenario not only such a signal would be visible by PAMELA but also be consistent with the increase of positrons measured by HEAT[57]. In conclusion a detailed measurement of the positron spectrum, its spectral features and its dependence from solar modulation will either provide evidence for a dark matter signature or strongly constrain and discard many existing models.

5.2 Galactic Cosmic Rays

Proton and electron spectra will be measured in detail with PAMELA . Also light nuclei (up to O) are detectable with the scintillator system. In this way it is possible to study with high statistics the secondary/primary cosmic ray nuclear and isotopic abundances such as B/C, Be/C, Li/C and $^3He/^4He$. These measurements will constrain existing production and propagation models in the galaxy, providing detailed information on the galactic structure and the various mechanisms involved.

5.3 Solar modulation of GCR

Launch of PAMELA occurred in the recovery phase of solar minimum with negative polarity (qA¡0) toward solar maximum of cycle 24. We are currently in an unusually long solar minimum with disagreement over prediction on the behavior of the intensity and peaking time of next maximum. In this period PAMELA has been observing solar modulation of galactic cosmic rays during decreasing solar activity. A long term measurement of the proton, electron and nuclear flux at 1 AU can provide information on propagation phenomena occurring in the heliosphere. As already mentioned, the possibility to identify the antiparticle spectra will allow to study also charge dependent solar modulation effects. In Figure 14 are shown the proton fluxes measured in various periods of the solar minimum. It is possible to see how the effect of decreasing solar activity on the flux of cosmic rays is visible even during this solar quiet period, in agreement with the increase of neutron monitor fluxes. Future work will involve correlation of the particle flux and solar modulation with variation with time of tilt angle.

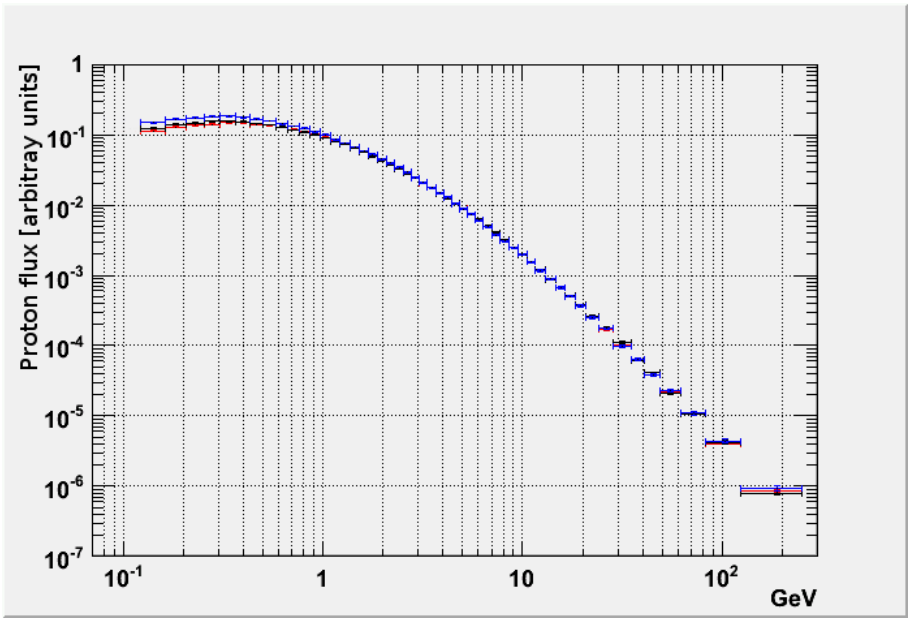

Figure 14: Differential spectrum of protons measured in July 2006 (red), January 2007 (black), August 2008 (blue). Below 1 GeV it is possible to see the flux variation due to solar modulation.

5.4 **Trapped particles in the Van Allen Belts**

The 70^o orbit of the Resurs-DK1 satellite allows for continuous monitoring of the electron and proton belts. The high energy ($> 80MeV$) component of the proton belt, crossed in the South Atlantic region will be monitored in detail with the magnetic spectrometer. Using the scintillator counting rates it will be possible to extend measurements of the particle spectra to lower energies using the range method. Montecarlo simulations have shown that the coincidence of the two layers of the topmost scintillator (S1) allows PAMELA to detect e^- from 3.5 MeV and p from 36 MeV. Coincidence between S1 and the central scintillator (S2) allows us to measure integral spectra of 9.5 e^- and 63 MeV p. In this way it will be possible to perform a detailed mapping of the Van Allen Belts showing spectral and geometrical features. Also the neutron component will be measured, although some care needs to be taken to estimate the background coming from proton interaction with the main body of the satellite. In Figure 15 is shown the differential energy spectrum

measured in different regions of the South Atlantic Anomaly. It is possible to see flux increase toward the centre of the anomaly. Particle flux exceeds several orders of magnitude the flux of secondary (reentrant albedo) particles measured in the same cutoff region outside the anomaly and is maximum where the magnetic field is lowest. However this is not the location of the flux at lowest energies according to scintillator counting rate. The reason for this difference is currently under investigation with comparison with existing models[18 58 59].

5.5 Secondary particles production in the Earth's atmosphere

To clearly separate primary component from the reentrant albedo (particles produced in interactions of cosmic rays with the atmosphere below the cutoff and propagating on Earth's magnetic field line) component it is necessary to evaluate the local geomagnetic cutoff. This is estimated using IGRF magnetic field model along the orbit; from this the McIlwain L shell is calculated[60]. In this work we have used the vertical Stormer (defined as $G = 14.9/L^2$) approximation[61]. Figure 10 shows the rigidity of particles as function of the evaluated cutoff G. The primary (galactic) component, with rigidities above the cutoff is clearly separated from the reentrant albedo (below cutoff) component, containing also trapped protons in the SAA. Note that color code shows the absolute value of β so that negative rigidity particles in the SAA region are albedo ($\beta < 0$ protons) with negative curvature in the tracker due to the opposite velocity vector. In Figure 16 is shown the particle flux measured at different cutoff regions. It is possible to see the primary (above cutoff) and the secondary (reentrant albedo - below cutoff) component. At the poles, where cutoff is below the detection threshold of PAMELA the secondary component is not present. Moving toward lower latitude regions the cutoff increases and it is possible to see the two components, with the position of the gap increasing with the increase of the cutoff. An accurate measurement of the secondary component is of relevance both in the calculation of the atmospheric neutrino [62 63] flux and in the estimation of hadronic cross sections (protons on O or N) at high energies, not otherwise determinable on ground.

5.6 **Solar energetic particles**

PAMELA observations are taking place at solar minimum, where about 10 significant solar events are expected during the three years experiment's lifetime [61]. The observation of solar energetic particle (SEP) events with a magnetic spectrometer will allow several aspects of solar and heliospheric cosmic ray physics to be addressed for the first time.

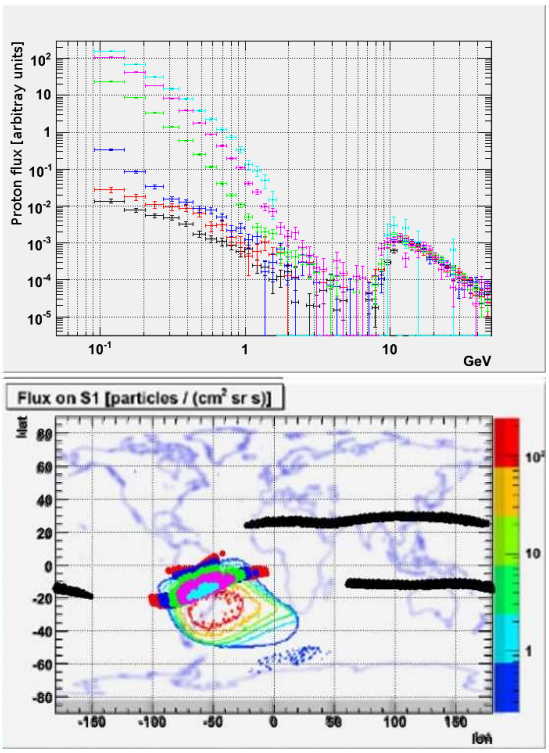

Figure 15: Top: Plot of the differential energy spectrum of PAMELA in different regions of the South Atlantic Anomaly. Regions are selected according to different intensity of the magnetic field (Black $B > 0.3G$ - outside the SAA, Red $0.22G < B < 0.23G$ Blue $0.21G < B < 0.22G$ Green $0.20G < B < 0.21G$ Pink $0.19G < B < 0.20G$ Turquoise $0.19G > B$) in the cutoff region $10.8GV < Cutoff < 11.5GV$. Trapped particles over the secondary particle flux measured in the same cutoff region outside the anomaly (black curve) are evident up to and above 1 GeV. Bottom: geographical regions corresponding to the above selection. The color bar corresponds to counting rate of the S1 (topmost) scintillator. Note the geographical shift between the peak of the SAA spectrum at high energy and the peak of the scintillator counting rate.

5.6.1 Electrons and Positrons

Positrons are produced mainly in the decay of π^+ coming from nuclear reactions occurring at the flare site. Up to now, they have only been measured indirectly

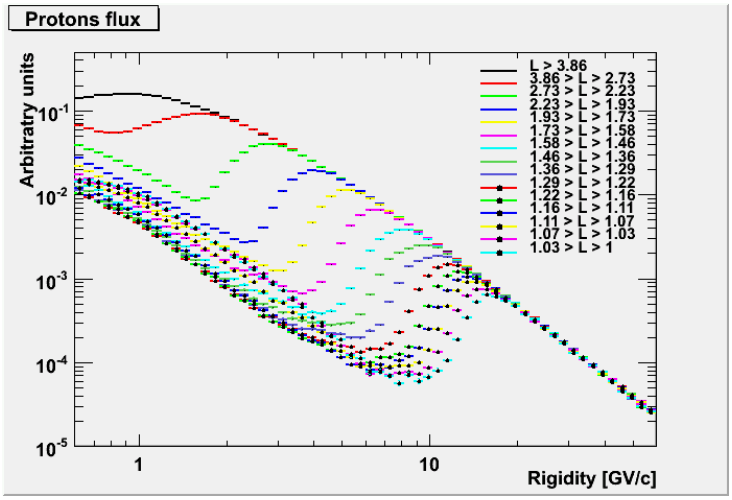

Figure 16: Plot of the differential energy spectrum of PAMELA at different L shells (according to McIlwain parameter). It is possible to see the primary spectrum at high rigidities and the reentrant albedo (secondary) flux at low rigidities. The transition between primary and secondary spectra is lower at lower cutoffs.

by remote sensing of the gamma ray annihilation line at 511 keV. Using the magnetic spectrometer of PAMELA it will be possible to separately analyze the high energy tail of the electron and positron spectra at 1 Astronomical Unit (AU) obtaining information both on particle production and charge dependent propagation in the heliosphere in perturbed conditions of Solar Particle Events.

5.6.2 Protons

PAMELA is capable to measure the spectrum of cosmic-ray protons from 80 MeV up to almost 1 TeV and therefore will be able to measure the solar component over a very wide energy range (where the upper limit will be limited by size and spectral shape of the event). These measurements will be correlated with other instruments placed in different points of the Earth's magnetosphere to give information on the acceleration and propagation mechanisms of SEP events. Up to now there has been no direct measurement[64] of the high energy (>1 GeV) proton component of SEPs. The importance of a direct measurement of this spectrum is related to the fact[65] that there are many solar events where the energy of protons is above the highest ($\simeq$100 MeV) detectable energy range of current spacecrafts, but is below the detection

threshold of ground Neutron Monitors[66]. However, over the PAMELA energy range, it will be possible to examine the turnover of the spectrum, where we find the limit of acceleration processes at the Sun.

5.6.3 Nuclei

PAMELA can identify light nuclei up to Carbon and isotopes of Hydrogen and Helium. Thus we can investigate the light nuclear component related to SEP events over a wide energy range. This should contribute to establish whether there are differences in the composition of the high energy (1 GeV) ions to the low energy component ($\simeq$ 20 MeV) producing γ rays or the quiescent solar corona[67]. These measurements will help us to better understand the selective acceleration processes in the higher energy impulsive[68] events.

5.6.4 Lowering of the geomagnetic cutoff

The high inclination of the orbit of the Resurs-DK1 satellite will allow PAMELA to study[69 70] the variations of cosmic ray geomagnetic cutoff due to the interaction of the SEP events with the geomagnetic field.

5.6.5 13 December 2006 Solar Particle event

At the time of writing the most significant events detected by PAMELA occurred between December 6^{th} and 17^{th} 2006 and were originated from region 930. Dec 6^{th} event was originated in the East, resulting in a gradual proton event reaching Earth on Dec 7^{th} and lasting until the events of Dec 13 and 14 [71]. On 13 December 2006, 02:38 UT an X3.4/4B solar flare occurred in active region NOAA 10930 ($S06^oW23^o$). The interaction between the fast rotating sunspot and the ephemeral regions triggers continual brightening and finally produces the major flare[72]. The intensity of the event (the second largest GLE of cycle 23) is quite unusual for a solar minimum condition. Starting at 2:50 UT on December 13, 2006, various neutron monitors, with cutoff rigidities below about $4.5\,GV$, recorded a Ground Level Enhancement (GLE70) with relative increases ranging from 20% up to more than 80% (Apaty, Oulu)[73 74]. Apaty and Oulu also registered the peak of the event beetween 02:40 UT and 03:10 UT, while most of the neutron monitors had it between 03:10 UT and 03:40 UT. The spectrum and its dynamic was investigated at higher energies using ground measurements by neutron monitors at different cutoff rigidities[75] resulting in a spectral estimation of $\gamma = 6$. The onset time was later for the proton channels on-board of GOES-11 satellite: 03:00 UT for greater than 100 MeV protons and 03:10 for greater than 10 MeV protons[74]. PAMELA was in an high cutoff region at the flare occurrence and reached the South Polar region at about 03:10 UT. Muon monitors were also able to detect the GLE event

and its spatial-angular anisotropy has been measured[76]. Differential proton spectra were directly meausured by GOES, ACE, Stereo, SAMPEX at energies below $400\,MeV$. With these instruments it was also possibile to measure the elemental composition of the various events[77 78].

The event produced also a full-halo Coronal Mass Ejection (CME) with a projected speed in the sky of 1774 km/s[79]. The forward shock of the CME reached Earth at 14:38 UT on December 14, causing a Forbush decrease of galactic cosmic rays which lasted for several days. A second SPE of lower intensity and energy occurred in conjunction with a X1.5 flare from the same active region (NOAA 10930, $S06^oW46^o$). A fourth event was observed at 17:23 UT on December 16 by ACE with the downstream passage of the CME. In Figure 17 is shown the differential energy spectrum measured with PAMELA in different periods of the event of the 13 December. It is possible to see that the event produced accelerated particles up to 3-4 GeV. A second smaller event occurred on Dec 14, superimposing on the Forbush decrease caused by the Coronal Mass Ejection of the previous event reaching Earth. Galactic particle flux thus decreased in the energy range up to 3 GeV, whereas solar particles were accelerated up to 1 GeV for this event. The decrease was also observed by Wind, Stereo and Polar but not by the GOES satellites, with the exception of some variation in the 15-40 MeV channell of GOES-12[80]. The relative decrease record by PAMELA was up to 20%, depending on the energy.

5.7 High energy lepton component

The calorimeter can provide an independent trigger to PAMELA for high energy releases due to showers occurring in it: a signal is generated with the release of energy above 150 mip in all the 24 views of planes from 7 to 18. With this requirement the geometrical factor of the calorimeter self-trigger is 400 cm^2sr if events coming from the satellite are rejected. In this way it is possible to study the electron and positron flux in the energy range between 300 GeV and 2 TeV, where measurements are currently scarce[81]. At this energy discrimination with hadrons is performed with topological and energetic discrimination of the shower development in the calorimeter coupled with neutron information coming from the neutron detector. This is because neutron production cross-section in an e.m. cascade is lower than in a hadronic cascade[82].

6 Conclusions

PAMELA was successfully launched on June 2006 and is currently operational in Low Earth Orbit. The satellite and the detectors are functioning correctly. It it expected that data from PAMELA will provide information on several items of cosmic ray physics, from antimatter to solar and trapped particles.

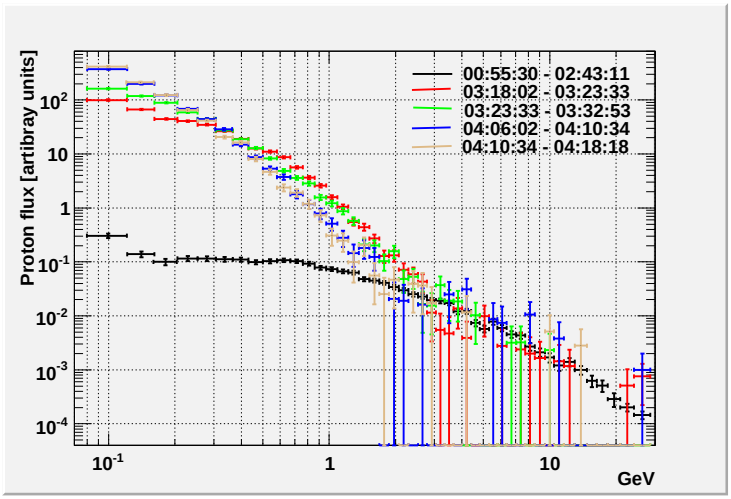

Figure 17: Proton differential energy spectra in different time intervals during the event of the 13th December 2006. The black line is the spectrum before the arrival of the charged particles with a small peak at low energy due to the presence of solar protons from previous events. It can be observed that the maximum flux of the high energy component of the solar protons arrives at the beginning of the event while only one hour later the maximum flux at low energy is detected. On the other hand, the flux at high energy decreases faster than at low energy.

References

1 . M. Boezio, et al., The Cosmic-Ray Antiproton Flux between 0.62 and 3.19 G eV Measured Near Solar Minimum Activity, ApJ 487 (1997) 415–+.

2 . M. Boezio, et al., The Cosmic-Ray Electron and Positron Spectra Measured at 1 AU during Solar Minimum Activity, ApJ 532 (2000) 653–669.

3 . V. Bidoli, et al., In-Orbit Performance of the Space Telescope NINA and Galactic Cosmic-Ray Flux Measurements, ApJS 132 (2001) 365–375.

4 . V. Bidoli, et al., Isotope composition of secondary hydrogen and helium above the atmosphere measured by the instruments NINA and NINA-2, Journal of Geophysical Research (Space Physics) 108 (2003) 1211–+.

5 . M. Casolino, et al., Space travel: Dual origins of light flashes seen in space, Nature 422 (2003) 680–+.

6 . V. Bidoli, et al., In-flight performance of SilEye-2 experiment and cosmic ray abundances inside the Mir space station, Journal of Physics G Nuclear Physics 27 (2001) 2051–2064.

7 . M. Casolino, et al., Detector response and calibration of the cosmic-ray detector of the Sileye-3/Alteino experiment, Advances in Space Research 37 (2006) 1691–1696.

8 . P. Picozza, et al., PAMELA - A payload for antimatter matter exploration and light-nuclei astrophysics, Astroparticle Physics 27 (2007) 296–315.

9 . M. Casolino, et al., The PAMELA Storage and Control Unit, Advances in Space Research 37 (2006) 1857–1861.

10 . M. Casolino, et al., YODA++: A proposal for a semi-automatic space mission control, Advances in Space Research 37 (2006) 1884–1888.

11 . http://www.samspace.ru/eng.

12 . http://eng.ntsomz.ru.

13 . G. Barbarino, et al., The PAMELA time-of-flight system: status report, Nuclear Physics B Proceedings Supplements 125 (2003) 298–302.

14 . O. Adriani, et al., The magnetic spectrometer of the PAMELA satellite experiment, Nuclear Instruments and Methods in Physics Research A 511 (2003) 72–75.

15 . M. Boezio, et al., A high granularity imaging calorimeter for cosmic-ray physics, Nuclear Instruments and Methods in Physics Research A 487 (2002) 407–422.

16 . S. Orsi, et al., The anticoincidence shield of the PAMELA space experiment, Advances in Space Research 37 (2006) 1853–1856.

17 . M. Pearce, et al., The Anticounter System of the PAMELA Space Experiment, in: International Cosmic Ray Conference, Vol. 4 of International Cosmic Ray Conference, 2003, pp. 2125–+.

18 . J. D. Gaffey, Jr., et al., NASA/National Space Science Data Center trapped radiation models, Journal of Spacecraft and Rockets 31 (1994) 172–176.

19 . On Behalf Of The Pamela Collaboration, M. Casolino, P. Picozza, On behalf of the PAMELA collaboration, Launch and commissioning of the PAMELA experiment on board the Resurs-DK1 satellite, Advances in Space Research 41 (2008) 2064–2070.

20 . V. di Felice, M. Casolino, N. de Simone, P. Picozza, PAMELA observational capabilities of Jovian electrons, Advances in Space Research 41 (2008) 2037–2042.

21 . On Behalf Of The Pamela Collaboration, M. Casolino, P. Picozza, On Behalf of the PAMELA collaboration, The PAMELA experiment: A spaceborne observatory for heliospheric phenomena, Advances in Space Research 41 (2008) 2043–2049.

22 . Y. Asaoka, et al., Measurements of Cosmic-Ray Low-Energy Antiproton and Proton Spectra in a Transient Period of Solar Field Reversal, Physical Review Letters 88 (5) (2002) 051101–+.

23 . M. Aguilar, et al., The alpha magnetic spectrometer (ams)on the international space station : Part i - results from the test flight on the space shuttle.

24 . M. Boezio, et al., The Cosmic-Ray Antiproton Flux between 3 and 49 GeV, ApJ 561 (2001) 787–799.

25 . S. Orito, et al., Precision Measurement of Cosmic-Ray Antiproton Spectrum, Physical Review Letters 84 (2000) 1078–1081.

26 . M. Hof, et al., Measurement of Cosmic-Ray Antiprotons from 3.7 to 19 GeV, ApJ467 (1996) L33+.

27 . J. W. Mitchell, et al., Measurement of 0.25-3.2 GeV Antiprotons in the Cosmic Radiation, Physical Review Letters 76 (1996) 3057–3060.

28 . M. Simon, et al., A New Calculation of the Interstellar Secondary Cosmic-Ray Antiprotons, ApJ 499 (1998) 250–+.

29 . L. Bergström, P. Ullio, private communication (1999).

30 . L. Bergström, et al., Cosmic Antiprotons as a Probe for Supersymmetric Dark Matter?, ApJ 526 (1999) 215–235.

31 . R. L. Golden, et al., Observation of cosmic ray positrons in the region from 5 to 50 GeV, A&A188 (1987) 145–154.

32 . D. Mueller, et al., Cosmic-ray positrons from 10 to 20 GeV - A balloon-borne measurement using the geomagnetic east-west asymmetry, ApJ 312 (1987) 183–194.

33 . J. M. Clem, et al., Solar Modulation of Cosmic Electrons, ApJ464 (1996) 507–+.

34 . R. L. Golden, et al., Observations of cosmic-ray electrons and positrons using an imaging calorimeter, ApJ 436 (1994) 769–775.

35 . R. L. Golden, et al., Measurement of the Positron to Electron Ratio in Cosmic Rays above 5 GeV, ApJ457 (1996) L103+.

36 . S. W. Barwick, et al., The Energy Spectra and Relative Abundances of Electrons and Positrons in the Galactic Cosmic Radiation, ApJ 498 (1998) 779–+.

37 . J. Alcaraz, et al., Leptons in near earth orbit, Physics Letters B 484 (2000) 10–22.

38 . M. Boezio, et al., Measurements of cosmic-ray electrons and positrons by the Wizard/CAPRICE collaboration, Advances in Space Research 27 (2001) 669–674.

39 . J. J. Beatty, et al., New Measurement of the Cosmic-Ray Positron Fraction from 5 to 15GeV, Physical Review Letters 93 (24) (2004) 241102–+.

40 . R. J. Protheroe, On the nature of the cosmic ray positron spectrum, ApJ 254 (1982) 391–397.

41 . I. V. Moskalenko, et al., Production and Propagation of Cosmic-Ray Positrons and Electrons, ApJ 493 (1998) 694–+.

42 . E. A. Baltz, et al., Positron propagation and fluxes from neutralino annihilation in the halo, Physical Review D59 (2) (1999) 023511–+.

43 . S. Profumo, et al., The role of antimatter searches in the hunt for supersymmetric dark matter, Journal of Cosmology and Astro-Particle Physics 7 (2004) 6–+.

44 . P. Ullio, Signatures of exotic physics in antiproton cosmic ray measurements, ArXiv Astrophysics e-prints.

45 . F. Donato, et al., Antiprotons in cosmic rays from neutralino annihilation, Phys.Rev.D 69 (6) (2004) 063501–+.

46 . A. M. Lionetto, et al., Uncertainties of cosmic ray spectra and detectability of antiproton mSUGRA contributions with PAMELA, Journal of Cosmology and Astro-Particle Physics 9 (2005) 10–+.

47 . K. M. Belotsky, et al., Composite dark matter and its charged constituents, Gravitation and Cosmology 12 (2006) 93–99.

48 . K. M. Belotsky, et al., May heavy neutrinos solve underground and cosmic-ray puzzles?, Physics of Atomic Nuclei 71 (2008) 147–161.

49 . M. Cirelli, et al., Minimal Dark Matter predictions for galactic positrons, anti-protons, photons, ArXiv e-prints 802.

50 . K. Abe, et al., Measurement of cosmic-ray low-energy antiproton spectrum with the first BESS-Polar Antarctic flight, ArXiv e-prints 805.

51 . H. Miyasaka, et al., Cosmic Ray Produced Antiprotons Confined in the Innermost Magnetosphere, in: International Cosmic Ray Conference, Vol. 7 of International Cosmic Ray Conference, 2003, pp. 4265–4268.

52 . D. Hooper, E. A. Baltz, Strategies for Determining the Nature of Dark Matter, ArXiv e-prints 802.

53 . D. Hooper, et al., Searching for dark matter with future cosmic positron experiments, Physical Review D71 (8) (2005) 083503–+.

54 . D. Hooper, et al., Kaluza-Klein dark matter and the positron excess, Phys.Rev.D 70 (11) (2004) 115004–+.

55 . M. Asano, et al., Cosmic positron signature from dark matter in the littlest Higgs model with T parity, Physical Review D75 (6) (2007) 063506–+.

56 . J. Hisano, et al., Heavy wino-like neutralino dark matter annihilation into antiparticles, Physical Review D73 (5) (2006) 055004–+.

57 . S. W. Barwick, et al., Measurements of the Cosmic-Ray Positron Fraction from 1 to 50 GeV, ApJ 482 (1997) L191+.

58 . R. S. Selesnick, et al., A theoretical model of the inner proton radiation belt, Space Weather 5 (2007) S04003.

59 . R. S. Selesnick, et al., Geomagnetically trapped antiprotons, Geophysical Research Letters34 (2007) 20104–+.

60 . Igrf-10 coefficients, Tech. rep., IAGA (2005).

61 . M. A. Shea, et al., Estimating cosmic ray vertical cutoff rigidities as a function of the McIlwain L-parameter for different epochs of the geomagnetic field, Physics of the Earth and Planetary Interiors 48 (1987) 200–205.

62 . M. Honda, et al., New calculation of the atmospheric neutrino flux in a three-dimensional scheme, Physical Review D70 (4) (2004) 043008–+.

63 . T. Sanuki, et al., Study of cosmic ray interaction model based on atmospheric muons for the neutrino flux calculation, Physical Review D75 (4) (2007) 043005–+.

64 . L. I. Miroshnichenko (Ed.), Solar Cosmic Rays, Vol. 260 of Astrophysics and Space Science Library, 2001.

65 . J. M. Ryan, Long-Duration Solar Gamma-Ray Flares, Space Science Reviews 93 (2000) 581–610.

66 . G. A. Bazilevskaya, et al., On The Stratospheric Measurements of Cosmic Rays, Space Science Reviews 85 (1998) 431–521.

67 . J. M. Ryan, Solar emissions (SH-1), in: International Cosmic Ray Conference, Vol. 10 of International Cosmic Ray Conference, 2005, pp. 357–+.

68 . D. V. Reames, Particle acceleration at the Sun and in the heliosphere, Space Science Reviews 90 (1999) 413–491.

69 . R. C. Ogliore, et al., A direct measurement of the geomagnetic cutoff for cosmic rays at space station latitudes, in: International Cosmic Ray Conference, Vol. 10 of International Cosmic Ray Conference, 2001, pp. 4112–4115.

70 . R. A. Leske, et al., Observations of geomagnetic cutoff variations during solar energetic particle events and implications for the radiation environment at the Space Station, Journal of Geophysical Research 106 (2001) 30011–30022.

71 . D. Wilkinson, Goes sem data summary 2006, Tech. rep., NOAA's National Geophysical Data Center (2006).

72 . J. Zhang, et al., Interaction between a Fast Rotating Sunspot and Ephemeral Regions as the Origin of the Major Solar Event on 2006 December 13, ApJl 662 (2007) L35–L38.

73 . J. W. Bieber, et al., A Maverick GLE: The Relativistic Solar Particle Event of December 13, 2006, in: ICRC 2007 Proceedings.

74 . Y. Q. Tang, Study of the ground level enhancement of 13 December 2006, in: ICRC 2007 Proceedings.

75 . E. Vashenyuk, et al., The GLE of December 13, 2006 according to the ground level and balloon observations, in: ICRC 2007 Proceedings.

76 . D. A. Timashkov, et al., Ground-Level Enhancement of December 13, 2006 in muon hodoscopes data, in: ICRC 2007 Proceedings.

77 . R. A. Mewaldt, et al., Observations of the December 2006 solar energetic particle events with the Low Energy Telescope (LET) on STEREO, in: ICRC 2007 Proceedings.

78 . C. M. S. Cohen, et al., Comparing observations and expectations of SEP composition in the two December 2006 events, in: ICRC 2007 Proceedings.

79 . Y. Liu, et al., A Comprehensive View of the 13 December 2006 CME: From the Sun to Interplanetary Space, ArXiv e-prints 802.

80 . T. Mulligan, et al., Unusual solar energetic proton fluxes at 1 AU within an interplanetary CME, in: ICRC 2007 Proceedings.

81 . T. Kobayashi, et al., in: 26^th Int. Cosm. Ray Conf., Salt Lake City, Vol. 3 61, 1999.

82 . A. Galper, Measurement of primary protons and electrons in the energy range of $10^{11} - 10^{13}$ ev in the pamela experiment, in: Proceedings ICRC, 2001.